Cold Chain Resilience Across Humanitarian and Resource-Constrained Settings: A Hybrid Simulation Framework

Arpish R. Solanki*[1]

[1]*Independent Researcher*

Preprint

Abstract

Cold chain systems are vital for preserving vaccines and other temperature-sensitive medicines, but in fragile, resource-constrained, and crisis-affected settings, they remain highly vulnerable to power instability, damaged infrastructure, and extreme climates. Existing modeling approaches commonly capture supply flows but overlook the interaction of thermal, logistical, and behavioral stressors that influence real-world resilience.

This study introduces a hybrid simulation framework that integrates physics-based refrigeration dynamics, power variability, logistics processes, agent behavior, stochastic disruptions, and temperature-dependent spoilage evaluation. The framework was applied to four illustrative contexts: Gaza conflict-affected setting, Sudan rural conflict-affected setting, Nepal highlands setting, and Haiti post-earthquake setting.

Results reproduced realistic vulnerability patterns. Clinics consistently emerged as the weakest nodes, with larger temperature fluctuations and frequent downtime, while depots and warehouses maintained relative stability. Power instability was the dominant driver of thermal risk across all settings, overshadowing transport or behavioral factors. Interventions that improved grid stability or overall infrastructure reduced temperature excursions and downtime by up to 60%, whereas isolated equipment upgrades frequently had minimal or negative effects due to higher power consumption.

The results showed that cold chain resilience emerged from the interaction of environmental, infrastructural, and behavioral factors rather than equipment performance alone. The framework provides a flexible tool for stress-testing interventions and supports evidence-based and context-specific strategies to safeguard equitable access to essential medicines in vulnerable settings.

Keywords: Cold chain resilience, Humanitarian logistics, Hybrid simulation, Power reliability, Vaccine cold storage

1 Introduction

Cold chain systems are a critical component of global public health, ensuring the safe storage and distribution of temperature-sensitive medical products like vaccines, insulin, and biologics [1, 2]. Yet nearly 1 billion people worldwide rely on health facilities with no or unreliable electricity,

*Corresponding author: arpish.sol@gmail.com

and in sub-Saharan Africa only 40% of facilities have reliable power [3, 4]. This energy gap directly threatens vaccine refrigeration, as well as oxygen concentrators and laboratory services. The World Health Organization (WHO) estimates that most routine Expanded Programme on Immunization (EPI) vaccines must be stored at 2–8°C, with only a few exceptions such as controlled temperature chain (CTC)-approved vaccines or ultra-cold mRNA products. When refrigeration fails, entire shipments may be lost [5–7], which disrupts immunization campaigns and wastes scarce health resources.

Global estimates of vaccine wastage vary widely, with WHO planning norms indicating 5–10% opened-vial wastage for preserved liquid vaccines and 30–50% for lyophilized multi-dose vaccines in routine immunization programmes [8]. Cold-chain failures are a common contributor to this loss. WHO reported that in 2011 alone, breakdowns in the cold chain across five countries led to the loss of approximately 2.8 million doses [9]. The consequences extend beyond numbers; lost doses mean missed vaccination courses and reduced protection in vulnerable populations [10–12]. For example, spoilage of 300,000 measles-rubella doses (two-dose schedule) could deprive 150,000 children of full protection. Failures also occur in high-income countries. In Ontario, Canada, a single clinic refrigerator malfunction in 2021 resulted in US $132,891.50 in spoiled vaccines, with system-wide losses estimated at over US $3 million annually [13, 14].

In fragile and crisis-affected settings, cold chain failures are especially acute. In April 2023, nationwide power outages amid conflict in Sudan ruined the national stock of insulin alongside vaccine reserves [15–17]. In 2019, health officials in Aden, Yemen, reported recurring vaccine spoilage due to electricity cut-offs [18]. In late 2021, authorities in Papua New Guinea halted the use of COVID-19 vaccine vials after excessive heat exposure during transport rendered them unusable [19]. In Gaza, the power situation deteriorated from an average of 13 blackout hours/day in early 2023 to a full electricity blackout from 11 October 2023, forcing hospitals onto scarce generator fuel and directly imperiling cold-chain equipment [20–22]. Beyond crises, national electrification remains uneven; a study by Mohammed et al. [23] reported that in 2022, only 49% of Sudan's rural population had electricity access, compared with 84% in urban areas, and conflict-related damage to power assets further undermines reliable energy for health services.

Environmental conditions compound these risks [24, 25]. Gaza regularly experiences summer highs around 30°C, with heatwaves exceeding 40°C [26, 27]. Sudan frequently records temperatures around 40°C during hot seasons, testing the limits of insulation and passive cooling [28]. By contrast, the Nepal Highlands face large daily swings, with warm days near 20–35°C in valleys but near-freezing nights at higher altitudes [29]. While Haiti averages 27–30°C with warm, humid nights, which compounds risks during disaster-induced outages [30].

Maintaining cold chain integrity in such contexts requires both systemic resilience and equipment performance. Energy reliability is often low, transport routes may be disrupted by damaged infrastructure or insecurity, and operational errors introduce additional risks. In these environments, failures rarely stem from a single weakness but from interactions among environmental, infrastructural, and human stressors [31–33].

A substantial body of research has addressed vaccine distribution and supply chain design, in particular through optimization and discrete-event simulation platforms such as HERMES, which were applied to redesign national and subnational EPI networks in settings like Mozambique and Niger [34–36]. These models capture stock flows, service coverage, and cost trade-offs under new vaccine introductions, and more recent COVID-19–era work has extended optimization

to account for evolving demand, multimodal delivery, and equity in distribution [37–39]. In parallel, agent-based models (ABM) have been used to explore humanitarian logistics problems such as warehouse siting, demand dynamics, and material convergence [40, 41], while resilience frameworks from WHO, UNICEF, and the broader supply chain literature provide conceptual tools for assessing capabilities and vulnerabilities [9, 42–45]. Similarly, stability models have predicted vaccine potency loss under temperature excursions using kinetic and statistical degradation approaches, including Arrhenius-based methods, accelerated predictive stability models, and mean kinetic temperature evaluations [46–48].

Despite this progress, thermal risk is generally oversimplified. Cold chain losses are often represented as fixed wastage rates or generic perishability [49], rather than modeled as outcomes of temperature excursions, power outages, holdover limits, or ambient heat exposure. Stability models generally relied on empirical or forced temperature profiles, rather than linking potency loss to infrastructure stressors or agent behavior. Similarly, although some ABM and resilience-oriented studies have addressed humanitarian logistics, they rarely integrated field-specific realities of crisis settings, such as blackouts, fuel scarcity, damaged roads, or security-related delays, let alone their direct thermal consequences on stored vaccines. Critically, we found no existing simulation framework that integrates agent behavior, infrastructure disruptions, environmental stressors, and thermal degradation into a unified model of cold chain performance and spoilage evaluation. As a result, operationally grounded cold chain simulations for humanitarian and disaster contexts remain rare.

This study addresses that gap by introducing a hybrid framework that combines physics-based refrigeration dynamics, energy system variability, human operational behavior, and stochastic disruptions. In simulation taxonomy, it is best described as a hybrid agent-based and physics-informed discrete-event framework. The framework is intended as a complementary analytical tool for exploring systemic resilience and thermal fragility, rather than a replacement for existing operational or logistics management systems.

In this study, the framework is applied to four contrasting operational contexts: Gaza (a densely populated, conflict-affected region with chronic power instability and disrupted transport networks), rural Sudan (a conflict-affected area characterized by sparse grid access, extreme heat, and limited refrigeration redundancy), the Nepal Highlands (a mountainous, remote setting with large day–night temperature swings and difficult terrain for transport), and post-earthquake Haiti (a disaster-affected tropical setting with prolonged grid outages and damaged infrastructure). Because these cases represent distinct combinations of environmental and infrastructure risks, they allow comparison of how cold chain resilience varies under different but equally difficult conditions. The objectives of this work are to introduce a hybrid simulation framework; simulate baseline cold chain performance under varied conditions; quantify impacts on system stability; and evaluate the relative effectiveness of technical, behavioral, and infrastructure-focused interventions.

2 Simulation Framework and Methods

The framework is structured as a discrete-time, agent-based simulation where time advances in fixed steps $t = 0, 1, 2, \ldots, T$. At each step, entities update synchronously in response to both internal logic and external conditions.

At the highest level, the cold chain is represented as a directed temporal graph. Nodes corre-

spond to warehouses, depots, or clinics, while edges represent transportation or transfer links. Each node hosts cold storage units with defined thermal properties and power dependencies and may also contain inventory and agents. Transfers are modeled as scheduled events moving inventory batches between nodes.

Inventory is organized into batches of temperature-sensitive items (e.g., vaccines, insulin), each governed by time- and temperature-dependent degradation models.

Heterogeneous agents carry out actions such as initiating deliveries, opening fridge doors, or repairing equipment. Their behavior can follow deterministic rules, probabilistic models, or scripted routines.

Environmental drivers such as ambient temperature and solar irradiance vary over time, while power availability is modeled separately for each node. These directly influence refrigeration and thus item stability.

Finally, the framework supports intervention scenarios. These can be applied at simulation start (static) or triggered dynamically by conditions during the run, allowing the system to test alternative policies and resilience strategies.

2.1 Environmental and Energy System Modeling

This simulation modeled the environmental context and energy availability that determined cold chain node performance. Each node operated under variable ambient conditions and drew power from a mix of sources. The parameters below governed the thermal and energetic dynamics of the system.

2.1.1 Ambient Temperature Dynamics

Ambient temperature $T_{\text{amb}}(t)$ was modeled as a hybrid deterministic–stochastic process to capture diurnal variation, inter-day variability, and rare anomalies. The daytime cycle was approximated as a cosine curve centered on solar noon:

$$T_{\text{amb}}(t) = \frac{T_{\text{day}} + T_{\text{night}}}{2} + \frac{T_{\text{day}} - T_{\text{night}}}{2} \cos\left(\frac{2\pi}{24}\,(t - t_{\text{noon}})\right),$$

where T_{day} and T_{night} are the daily maximum and minimum baseline temperatures, respectively, and t_{noon} denotes solar noon. Night and day baselines varied stochastically by ±1.5°C across simulated days.

After sunset, ambient cooling was modeled as exponential decay toward T_{night} with time constant τ:

$$T_{\text{amb}}(t + \Delta t) = T_{\text{night}} + \left(T_{\text{amb}}(t) - T_{\text{night}}\right) e^{-\Delta t/\tau}.$$

Occasional anomalies such as cold snaps or heat waves (±2°C) were introduced with probability $\approx 5\%$ per step.

This ambient model influenced both refrigeration heat exchange and solar energy generation.

2.1.2 Energy Source Modeling

Nodes could be configured with multiple energy sources. Power availability was modeled as a time-varying combination of the following:

Grid Power: Modeled as a binary availability flag $P_{\text{grid}}(t) \in \{0, 1\}$, controlled by predefined outage schedules or stochastic blackout processes. Forced shutdown events were also supported.

Solar Power: Output was given by

$$P_{\text{solar}}(t) = \eta_{\text{panel}}\, I(t)\, A_{\text{panel}}\, \alpha(\theta, \phi),$$

where $I(t)$ is solar irradiance (W/m^2), A_{panel} is panel area (m^2), η_{panel} is panel efficiency, and $\alpha(\theta, \phi)$ is an orientation/tilt correction factor ($0 \leq \alpha \leq 1$).

Battery Storage: The stored energy $B(t)$ (Wh) evolved as

$$B(t + \Delta t) = B(t) + \eta_{\text{ch}} P_{\text{in}}(t)\, \Delta t - \frac{1}{\eta_{\text{dis}}} P_{\text{out}}(t)\, \Delta t - \Delta E_{\text{degrade}},$$

where $P_{\text{in}}(t)$ and $P_{\text{out}}(t)$ are charging/discharging powers (W), η_{ch} and η_{dis} are charging/discharging efficiencies, and $\Delta E_{\text{degrade}}$ represents cumulative degradation losses. Capacity loss was modeled through cycle damage, temperature effects, and an additional weekly degradation rate.

Backup Generator: If present, the generator supplied power when other sources failed. Its availability was defined as

$$P_{\text{gen}}(t) = \begin{cases} P_{\text{rated}}, & F(t) > 0, \\ 0, & F(t) = 0, \end{cases}$$

where $F(t)$ is remaining fuel (L) and P_{rated} is the generator's rated output (W). Fuel could be replenished by agents during the simulation.

2.1.3 Power Management Logic

Nodes followed a fallback hierarchy to route power demand:

$$\text{Available Power} = \begin{cases} P_{\text{grid}}(t) & \text{if grid is available} \\ P_{\text{solar}}(t) & \text{if solar generation exceeds load} \\ P_{\text{battery}}(t) & \text{if sufficient charge remains} \\ P_{\text{gen}}(t) & \text{if fuel is available} \\ 0 & \text{otherwise.} \end{cases}$$

This priority model ensured continuity while limiting fuel and battery overuse. Configurations were node-specific.

2.2 Refrigeration Dynamics Modeling

The internal temperature of each cold storage unit (e.g., vaccine fridge) was modeled as the combined effect of passive heat exchange with the environment and active cooling when the compressor was engaged. The formulation follows Newton's Law of Cooling, adapted to a discrete-time framework with timestep Δt.

2.2.1 *Internal Temperature Model*

Let $T_{\text{fridge}}(t)$ denote the internal fridge temperature at time t, and $T_{\text{amb}}(t)$ the external ambient temperature. The next-step temperature $T_{\text{fridge}}(t + \Delta t)$ is modeled as:

$$T_{\text{fridge}}(t + \Delta t) = T_{\text{fridge}}(t) + \frac{\Delta t}{C_{\text{th}}} \left(\frac{T_{\text{amb}}(t) - T_{\text{fridge}}(t)}{R} + P_{\text{cool}}(t) \right) + \frac{Q_{\text{door}}(t) + Q_{\text{mix}}(t)}{C_{\text{th}}},$$

where:

- R is the thermal resistance of the fridge insulation (K/W),
- C_{th} is the fridge thermal capacitance (J/K),
- $P_{\text{cool}}(t)$ is the cooling power applied at time t (W),
- $Q_{\text{door}}(t)$ is heat energy introduced by door openings during Δt (J),
- $Q_{\text{mix}}(t)$ is heat energy from incoming items (J).

This captures competing dynamics of environmental heat gain, compressor-driven cooling, and stochastic load disturbances. Door-opening events are generated by agent actions as described in Section 2.7.1, with stochastic timing determined by profile- and mode-dependent probabilities.

2.2.2 *Compressor Control and Power Consumption*

The compressor followed thermostat logic, activating when $T_{\text{fridge}}(t)$ exceeded an upper threshold T_{max} and switching off below a lower bound T_{min}:

$$s_{t+1} = \begin{cases} 1, & T_{\text{fridge}}(t) > T_{\text{max}}, \\ 0, & T_{\text{fridge}}(t) < T_{\text{min}}, \\ s_t, & \text{otherwise}, \end{cases}$$

where $s_t \in \{0, 1\}$ denotes compressor state. Cooling power was then:

$$P_{\text{cool}}(t) = \begin{cases} -P_{\text{cool,rated}}\, \eta_{\text{cool}}, & \text{if compressor active and powered}, \\ 0, & \text{otherwise}, \end{cases}$$

with $P_{\text{cool,rated}}$ the rated cooling capacity (W), and η_{cool} an efficiency factor.

2.3 Thermal Load Modifiers

Door-Opening Events: Each opening injected heat $Q_{\text{door}}(t)$ into the fridge; usage profiles governed stochastic door events.

Load-Exchange Effects: When items at temperature T_{item} were introduced, a transient mixing heat

$$Q_{\text{mix}}(t) = C_{\text{item}} \left[T_{\text{item}} - T_{\text{fridge}}(t) \right]$$

was added once in the main balance.

Thermal Buffering Capacity: Higher C_{th} slowed temperature fluctuations, buffering against outages and brief disturbances.

2.4 Product Stability and Spoilage Modeling

Cold chain inventory was modeled at both batch and item levels, with thermal and spoilage logic applied dynamically during the simulation. Each item corresponded to a temperature-sensitive medical product (e.g., vaccines, insulin), parameterized by thermophysical and degradation characteristics.

2.4.1 Batch and Item Representation

Each batch B_i consisted of multiple perishable items, each item defined as:

$$\text{Item}_j = \left(T_0, T_{\min}, T_{\max}, t_{\max}, \text{Model}, \text{Priority}, C\right)$$

- T_0: Initial temperature
- $T_{\min}, T_{\max}$: Safe storage range
- $t_{\max}$: Maximum cumulative unsafe exposure (hours)
- `Priority`: Criticality label (e.g., HIGH, MEDIUM)
- C: Thermal mass ($J/°\text{C}$), determining thermal inertia
- `Model`: Spoilage evaluation strategy (see below)

Each item tracked:

- Exposure history $\mathcal{E} = \{(\delta t_i, T_{\text{item},i})\}$ (pairs of duration and observed temperature),
- Accumulated unsafe time $\sum \delta t_i$,
- A spoilage flag, updated at each simulation step.

2.4.2 Spoilage Evaluation Models

Multiple mechanistic and statistical models were supported, selectable per item type.

1. Abrupt Model

Spoils immediately upon *any* unsafe exposure:

$$S = 1 \iff \exists (\delta t_i, T_{\text{item},i}) \in \mathcal{E} \text{ s.t. } T_{\text{item},i} \notin [T_{\min}, T_{\max}]$$

2. Cumulative Model

Spoils once the total unsafe exposure time exceeds a threshold:

$$S = 1 \iff \sum_{\{i \,|\, T_{\text{item},i} \notin [T_{\min}, T_{\max}]\}} \delta t_i \;\geq\; t_{\max} + \Delta t_{\text{buffer}}$$

3. Threshold Model

Spoils if a single continuous unsafe exposure exceeds the maximum allowable duration:

$$S = 1 \iff \exists(\delta t_i, T_{\text{item},i}) \text{ s.t. } T_{\text{item},i} \notin [T_{\min}, T_{\max}] \quad \wedge \quad \delta t_i \geq t_{\max}$$

4. Linear-Risk Model

Computes probabilistic spoilage from accumulated thermal severity:

$$\text{Risk} = \frac{1}{Z} \sum_{\{i \,|\, T_{\text{item},i} \notin [T_{\min}, T_{\max}]\}} \delta t_i \cdot \left| T_{\text{item},i} - T_{\text{safe}}^{\text{mid}} \right|$$

where Z is a normalization constant. Spoilage occurs if Risk $> U(0,1)$, with U a uniform random draw.

5. Thermal-Stress Model

Aggregates exposure-weighted stress:

$$\text{Stress} = \sum_{\{i \,|\, T_{\text{item},i} \notin [T_{\min}, T_{\max}]\}} \left| T_{\text{item},i} - T_{\text{safe}} \right| \cdot \delta t_i$$

Spoils if Stress exceeds a predefined threshold.

6. Arrhenius Model

Captures chemical degradation using Arrhenius kinetics:

$$k(T_{\text{item},i}) = A \cdot e^{-\frac{E_a}{R_u T_{\text{item},i}}}$$

At discrete steps δt_i, cumulative degradation progressed as:

$$\text{Progress} = \sum_i k(T_{\text{item},i}) \cdot \Delta t$$

Spoils if Progress ≥ 1.

Where:

- Δt: Simulation time interval,
- A: Pre-exponential factor,
- E_a: Activation energy,
- R_u: Universal gas constant,
- $T_{\text{item},i}$: Temperature at step t_i (in Kelvin).

2.5 Transport and Logistics Modeling

2.5.1 Transport Units

Each transport unit was modeled with thermal characteristics that determined its internal stability.

Thermal inertia: governed the rate at which internal temperature responded to external variation,

Insulation efficiency: controlled heat exchange with the ambient environment,

Passive cooling capacity: represented ice packs or phase-change materials (PCM) that temporarily stabilized conditions during transit.

The internal temperature $T_{\text{unit}}(t)$ of a transport unit evolved dynamically according to:

$$T_{\text{unit}}(t+1) = T_{\text{unit}}(t) + \frac{\Delta t}{C_{\text{unit}}} \cdot \frac{T_{\text{amb}}(t) - T_{\text{unit}}(t)}{R_{\text{unit}}} - \Delta T_{\text{passive}}(t),$$

where:

- C_{unit} is the thermal mass of the transport container,
- R_{unit} is the thermal resistance (insulation quality),
- $T_{\text{amb}}(t)$ is the ambient temperature at time t,
- $\Delta T_{\text{passive}}(t)$ is the effective cooling contribution from ice packs or PCM at time t.

At each timestep Δt, the heat inflow into the unit was

$$Q_{\text{in}}(t) = \frac{T_{\text{amb}}(t) - T_{\text{unit}}(t)}{R_{\text{unit}}} \cdot \Delta t,$$

where $T_{\text{amb}}(t)$ is the ambient temperature and R_{unit} the insulation thermal resistance.
The ice pack absorbed heat until depletion:

$$Q_{\text{ice}}(t + \Delta t) = \max\big(Q_{\text{ice}}(t) - Q_{\text{in}}(t),\ 0\big),$$

where $Q_{\text{ice}}(t)$ is the remaining latent energy in the icepack.
When $Q_{\text{ice}}(t) > 0$, the passive cooling contribution was sufficient to maintain stability. After complete melting, additional heat raised the internal temperature according to

$$T_{\text{unit}}(t + \Delta t) = T_{\text{unit}}(t) + \frac{Q_{\text{in}}(t)}{C_{\text{unit}}},$$

with C_{unit} the effective thermal mass of the transport container and its contents.

2.5.2 Shipment and Transfer Events

Logistical movements were represented as scheduled transfer events. Each event transported batches along a temporal edge in the logistics network:

$$\mathcal{T} = \big(t_{\text{dep}}, t_{\text{arr}}, u_{\text{origin}}, u_{\text{dest}}, U_{\text{container}}\big),$$

where t_{dep} and t_{arr} denote departure and arrival times, u_{origin} and u_{dest} are network nodes, and $U_{\text{container}}$ is the transport unit used.
The logistics network was represented as a temporal directed graph $\mathcal{G} = (V, E, T_{\text{avail}})$, where:

- V are cold chain nodes,
- E are directed transport links,
- T_{avail} encodes time-dependent availability of edges.

Batches moved along edges as temporal flows, with their state (temperature, spoilage flag, and exposure history) updated continuously according to the transport unit dynamics over the interval $[t_{\text{dep}}, t_{\text{arr}}]$.

2.6 Disruption and Failure Modeling

The system incorporated discrete stochastic events to represent disruptions in the cold chain environment. These included operational instabilities, infrastructure failures, and human-induced incidents. Each event was defined by a triggering condition and a set of time-dependent consequences.

Let $\mathcal{EV} = \{ev_1, ev_2, \ldots, ev_k\}$ denote the set of possible event types (e.g., power outage, battery theft, fridge tampering, transport delay).

Each event $ev \in \mathcal{EV}$ was represented as a time-stamped tuple:

$$ev = (t_{ev}, \text{target}, \text{effect}, \text{duration}, \text{metadata}),$$

where `target` identified the affected entity, `effect` described the disruption logic, and `duration` determined persistence.

Events were triggered by stochastic processes, typically modeled as Bernoulli trials with fixed or adaptive probabilities:

$$\Pr(ev \text{ at time } t) = p_{ev},$$

where p_{ev} could be constant or vary dynamically with regional indices or system state.

For example, battery theft at a depot could be triggered with probability p_{theft} per step. A blackout at a warehouse grid connection might occur with probability p_{blackout}, persisting for a duration $d \sim \text{Geom}(\lambda)$.

Event propagation was managed by a central scheduler, which queued and applied effects at the correct simulation time t, including overriding node or transport properties (e.g., disabling power), forcing thermal shifts (e.g., temperature rises), or canceling and delaying scheduled transfers.

Rare catastrophic disruptions (e.g., sabotage, tampering, looting) were modeled as low-probability triggers.

To ensure reproducibility, all events could be deterministically regenerated using seeded randomness, logs, or replay files that allows exact replication of disruption sequences.

Additional event types included human errors such as leaving fridge doors ajar or missing refueling and environmental variability such as reduced solar output. While most disruptions were treated as binary events, some (e.g., poor solar yield) were modeled as continuous modifiers to input rather than discrete failures. Grid blackouts could also follow scheduled outage windows.

2.7 Agent-Based Behavior Modeling

Human actors introduced operational variability into cold chain systems. Their behaviors were modeled as probabilistic processes, conditioned on environmental state variables or accumulated stress. Three primary agent types were included: health workers, technicians, and transport agents.

2.7.1 Health Worker Actions

Health workers interacted routinely with cold storage units. Agent behavior was characterized by two layers:

- Long-term behavioral profiles: $B_a \in \{\text{CAREFUL}, \text{MULTIUSE}, \text{CHAOTIC}\}$, representing general tendencies.
- Short-term modes: $M_a(t) \in \{\text{NORMAL}, \text{LAZY}, \text{HEROIC}, \text{BURNED\_OUT}\}$, which evolved dynamically in response to stressors.

Key modeled events included:
Fridge Access: The probability of a fridge door opening at time t was modeled as:

$$p_{\text{open,agent}}(t) = f_{\text{profile}}(B_a) \cdot f_{\text{mode}}(M_a(t)) \cdot f_{\text{context}}(T_{\text{amb}}(t), S(t)),$$

where $T_{\text{amb}}(t)$ is the ambient temperature and $S(t)$ the current power status.

Misuse under Stress: During prolonged outages or temperature excursions, agents could undertake maladaptive actions (e.g., relocating the fridge, opening the fridge during a power outage). This probability was modeled conditionally as follows.

$$p_{\text{misuse,agent}} = \Pr\big(\text{action} \,\big|\, T_{\text{unit}}(t) > \theta_T,\ B_a = \text{CHAOTIC}\big).$$

Door Event Process: Door openings were generated as profile-conditioned stochastic events with per-day limits:

$$N_{\text{open}}^{(B_a)} \approx \text{E}[\text{opens/day} \mid B], \qquad \Delta t_{\text{open}} \sim U[a_B, b_B],$$

where $N_{\text{open}}^{(B)}$ is the expected number of daily openings under profile B_a, and Δt_{open} is the event duration drawn from a uniform distribution. Each opening contributed a thermal ingress. Each stochastic door-opening event contributes heat $Q_{\text{door}}(t)$ to the fridge temperature dynamics (Section 2.3).

2.7.2 Technician Actions

Technicians managed equipment failures and backup power systems. Their reliability was modeled as follows:

Repair Success: Repairs were modeled as Bernoulli trials with probability $p_{\text{repair}}(M_a(t))$, dependent on the technician's mode. Failures triggered reattempts in subsequent timesteps, thereby increasing systemic risk.

Response Delay: The time between disruption occurrence and technician arrival was drawn from a Gamma distribution:

$$T_{\text{response}} \sim \text{Gamma}(\alpha, \beta),$$

where α is the shape parameter and β is the scale parameter. These parameters reflected contextual factors such as geography, transport reliability, and staffing.

Maintenance Reliability: Routine preventive tasks (e.g., generator refueling) could be neglected with probability $p_{\text{neglect}}(M_a(t))$, which increased downstream failure risk when neglected.

2.7.3 *Transport Agents and Delivery Uncertainty*

Each transfer was modeled as a discrete event. Transport reliability was captured through stochastic modifiers.

Arrival Delay: The actual arrival time was perturbed by a delay variable $\delta \sim \text{Exp}(\lambda_d)$, where λ_d represented regional transport reliability. In contexts with poor infrastructure, checkpoints, or fuel scarcity, a lower λ_d produced longer expected delays. The effective arrival time became

$$t_{\text{arr,actual}} = t_{\text{arr}} + \delta$$

Delivery Failure: Each transfer carried an independent probability of complete failure, $\Pr(\text{failure}) = p_{\text{fail,deliv}}$, representing disruptions such as roadblocks, theft, or missed schedules. Additional risks (e.g., looting, tampering, cascading instability) were modeled as separate stochastic events applied during the transfer process.

2.7.4 *Agent Mode Transitions*

Agents were modeled with dynamic behavioral states. Their modes evolved according to a hybrid stochastic process, a base first-order Markov chain, biased by recent events and cumulative stress exposure.

Formally, the probability of transitioning to a new mode $M_a(t+1)$ was given by

$$\Pr(M_a(t+1) \mid M_a(t), \Sigma_a(t), E_a(t)) \propto P_{B_a}(M_a(t)) + f(\Sigma_a(t), E_a(t)),$$

where

- P_{B_a} is the baseline transition probability row from the agent's profile-specific matrix B_a,
- $\Sigma_a(t)$ is the cumulative stress, and
- $E_a(t)$ is the subset of recent system-wide events affecting agent a:

$$E_a(t) \subseteq \mathcal{EV}$$

The biasing function $f(\cdot)$ adjusted the baseline probabilities (e.g., looting increased the likelihood of heroic responses, and repeated failures increased burnout). After adjustment, probabilities were renormalized to ensure a valid distribution. This hybrid design preserved the tractability of a Markov chain while introducing event-driven and stress-driven adaptability.

2.8 Scenario Design and Contexts

Four illustrative scenarios were developed to investigate cold chain resilience in different humanitarian contexts.

Gaza conflict-affected setting

This scenario serves as a high-temperature, conflict-affected environment with severe energy insecurity. Daily peaks reached the mid-30s°C, with only mild cooling at night. Grid availability was assumed to be extremely limited and represented with an hourly availability profile, supplemented by solar panels and small generators [50–53]. Cold chain units at warehouse, depot, and clinic levels were modeled with moderate insulation but limited reliability. Disruption

probabilities included frequent blackouts and transport delays [54, 55]. Transport included a mix of WHO-grade and locally built passive carriers.

Sudan rural conflict-affected setting

The Sudan setting captured extreme heat and fragile rural infrastructure characteristic of conflict-affected, resource-limited regions. Daytime highs exceeded 37°C, with warm nights. Cold chain equipment was assumed to be older and less efficient, particularly at the clinic level, where fridges had weak compressors and poor insulation. Grid access was unreliable, and repair times were modeled as highly delayed [56, 57]. Events included assumed roadblocks due to flooding, insecurity, or poor roads [58, 59]. Transport relied heavily on motorbikes and bicycles with small carriers.

Nepal highlands setting

The Nepal Highlands scenario reflected a cold-climate, mountainous context where terrain and altitude dominated logistical challenges. Ambient temperatures were cooler ($\approx$ 16 °C by day, near freezing at night), which decreased cooling demands but complicated transport. Compared to conflict settings, power reliability was higher; however, terrain and shade limited solar efficiency. Road closures and landslide-related transportation disruptions were more commonly assumed than blackouts [60, 61]. Transport units included porters, motorbikes, bike carts, and small vans adapted for mountainous terrain.

Haiti post-earthquake setting

The Haiti scenario represented a post-disaster setting following the earthquake in a country with an already weak and unreliable electricity grid [62]. Ambient conditions captured hot and humid tropical weather. Cold chain units at all levels were assumed to have higher insulation but faced extreme energy insecurity ($\approx$ 30% grid uptime). Event probabilities emphasized damaged infrastructure and supply bottlenecks. Transport relied on passive vans and carriers of moderate insulation quality.

Overall, these scenarios were illustrative stress tests based on assumed parameters informed by climatic, infrastructural, and contextual characteristics reported in humanitarian literature. They did not use official operational datasets from ministries or agencies, nor were they intended to replicate exact field conditions. Rather, the regional references guided assumptions on road accessibility, storage equipment quality, electricity reliability, and transportation availability, which allowed the simulation framework to be meaningfully evaluated across different crisis-affected environments. One clinic was purposefully deprived of regular delivery in order to represent service inequalities frequently seen in humanitarian contexts. For brevity, we refer to scenarios by geographic archetypes (for example, 'Sudan', 'Gaza'), although these are stylized archetypes rather than full national representations.

The full configuration files (YAML) used in these experiments will be made available with the simulation code repository on GitHub prior to publication. Configuration files include inline comments with rationale for parameter values.

To assess resilience-enhancing strategies, intervention scenarios were defined as structured modifications to the system's baseline parameters. Each intervention altered a subset of parameters $\Delta\Pi$, representing targeted changes in infrastructure, behavior, or operational logistics. Interventions were tested under each region's modeled constraints, with generator fuel capped at one full run. Interventions were evaluated individually and in pairwise combinations to explore independent and synergistic effects on cold chain performance. All interventions were labeled, recorded, and analyzed for comparability. A detailed list of parameter changes is

provided in Supplementary Tables S1-S4.

Sensitivity analysis was conducted to assess the robustness of outcomes to uncertain configuration parameters. One-at-a-time perturbations of ±30% were applied to key inputs. Each variant was repeated with three random seeds, and spoilage metrics were aggregated.

3 Results

Prior to running full scenarios, subsystem-level tests were conducted to confirm that discrete components behaved as expected. These included verifying that fridge temperatures rose after power cuts and door openings, that higher insulation slowed warming while ambient heat accelerated it, that batteries charged and discharged correctly from grid and solar inputs, that passive transport units depleted ice packs under prolonged exposure while motorized carriers maintained stability, and that outages depleted batteries and generator and triggered technician actions of refueling. Spoilage models also correctly flagged items exceeding unsafe exposure limits. All tests passed, confirming that subsystem dynamics behaved as intended before applying the framework to multi-node scenarios (Figure 1).

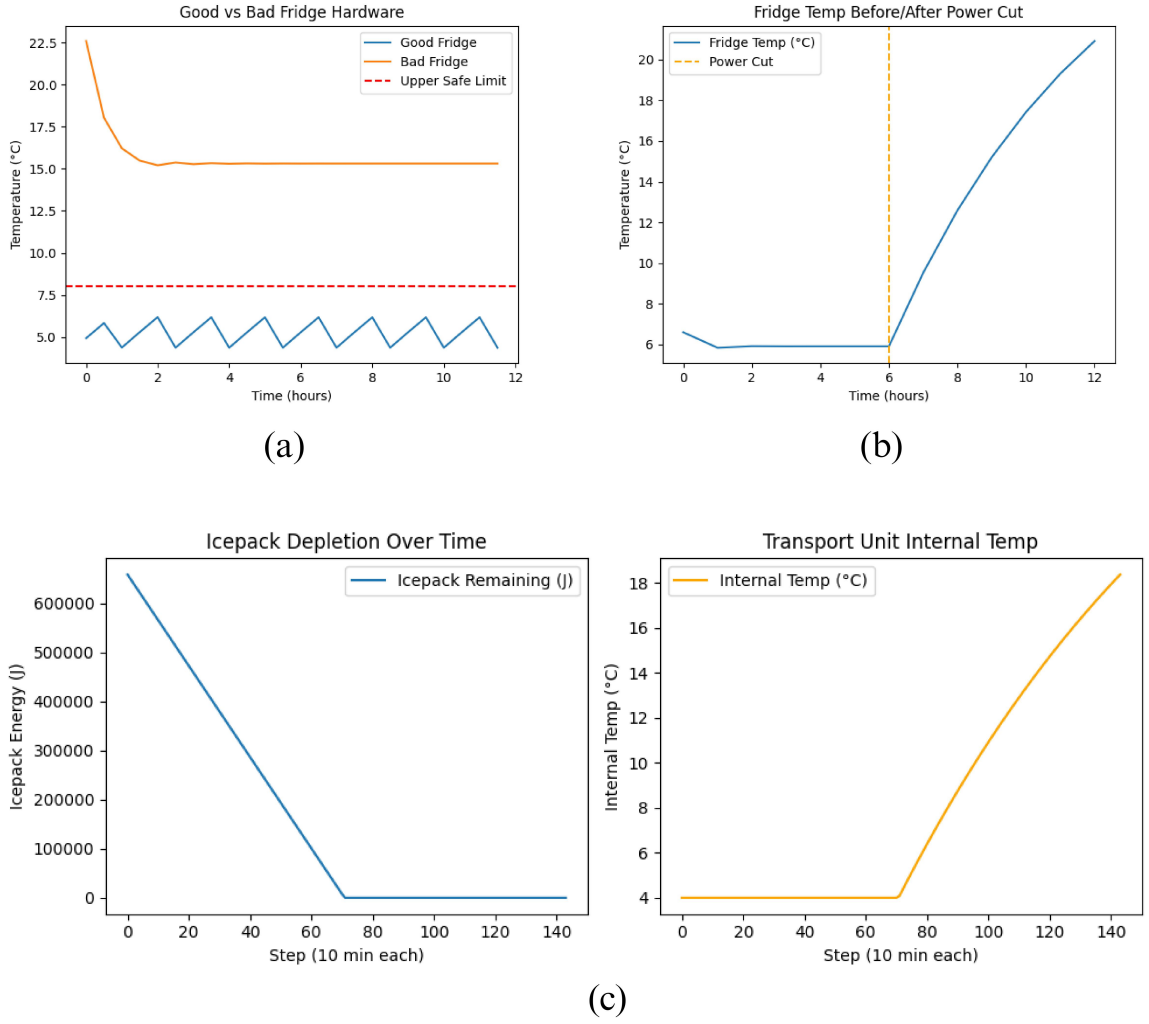

Figure 1: Subsystem verification. (a) Temperature stability in a high-insulation, high thermal mass, strong cooling ("good") vs. low-insulation, weak cooling, low thermal mass ("bad") fridge. (b) The fridge is warming following a power cut after stabilization at 5.5 °C. (c) Passive transport unit using ice packs, showing stable conditions until ice depletion, after which internal temperature rises toward ambient. These checks confirm that subsystem dynamics behave as expected before scenario-level experiments.

For most selected subsystem parameters, spoiling results remained relatively stable during ±30% parameter changes, with mean shifts <±0.02 compared to baseline. Refrigerator insulation and thermal mass, however, had a considerable impact; the spoiling fraction rose from 0.07 (improved +30%) to 0.73 (degraded -30%) (Figure 2).

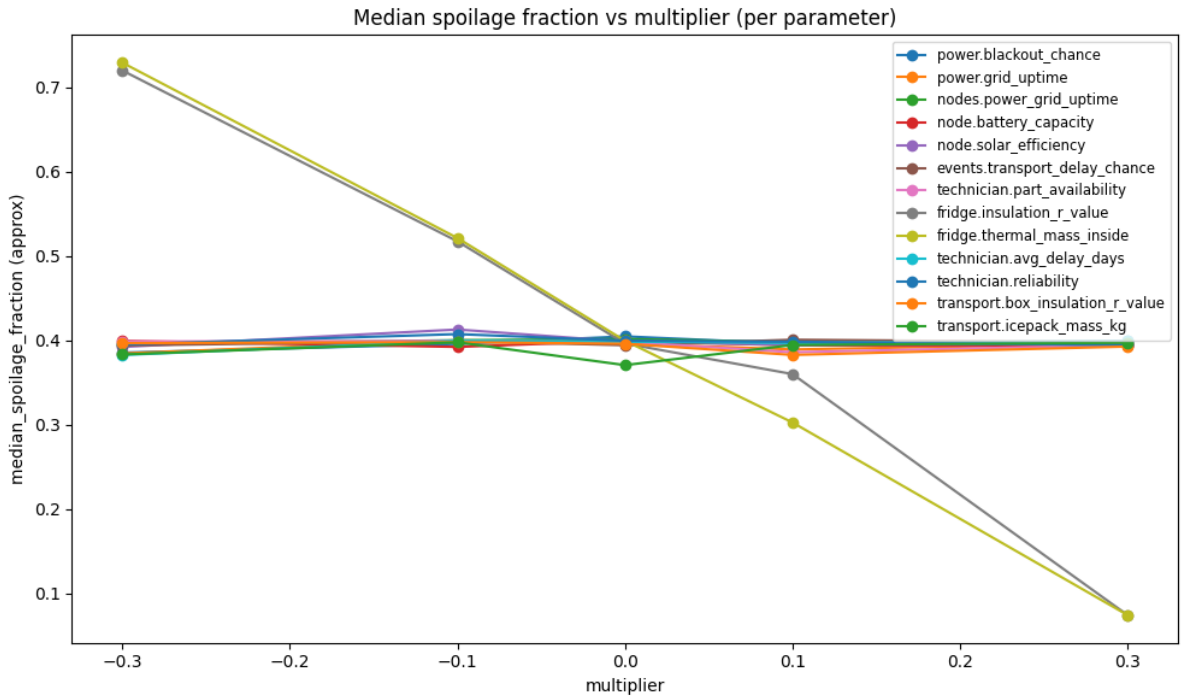

Figure 2: Spoilage fraction under ±30% perturbations of selected parameters. Fridge insulation and thermal mass show strong sensitivity, while others remain relatively stable.

The simulated refrigeration systems generally maintained internal temperatures within the WHO-recommended 2–8 °C range throughout the 72-hour baseline runs in Gaza, rural Sudan, the Nepal Highlands, and post-earthquake Haiti. Depots and warehouses exhibited greater stability than clinics, with warehouses averaging 4.4–4.7 °C compared to clinic means of 5.1–5.2 °C. Clinic-level fluctuations were most evident in Gaza and Sudan, driven by high ambient peaks, while Nepal and Haiti remained closer to mid-range stability despite large day–night swings and tropical heat respectively (Figure 3). Diurnal patterns were evident across all settings, with minor afternoon rises that were buffered by modeled insulation and thermal mass. In Gaza and Sudan, occasional excursions above 10 °C occurred in depots and warehouses once backup generators reached their modeled fuel cap.

Transport performance varied more widely. Motorbikes and vans with moderate insulation reliably maintained safe ranges in Gaza, Nepal, and Haiti, even under ambient peaks near 35 °C. By contrast, low-insulation passive units showed repeated breakdowns. In the Sudan scenario, the Bicycle1 unit peaked around 17 °C after ice depletion. Deliveries generally stabilized after ice pack replenishment (Figure 4).

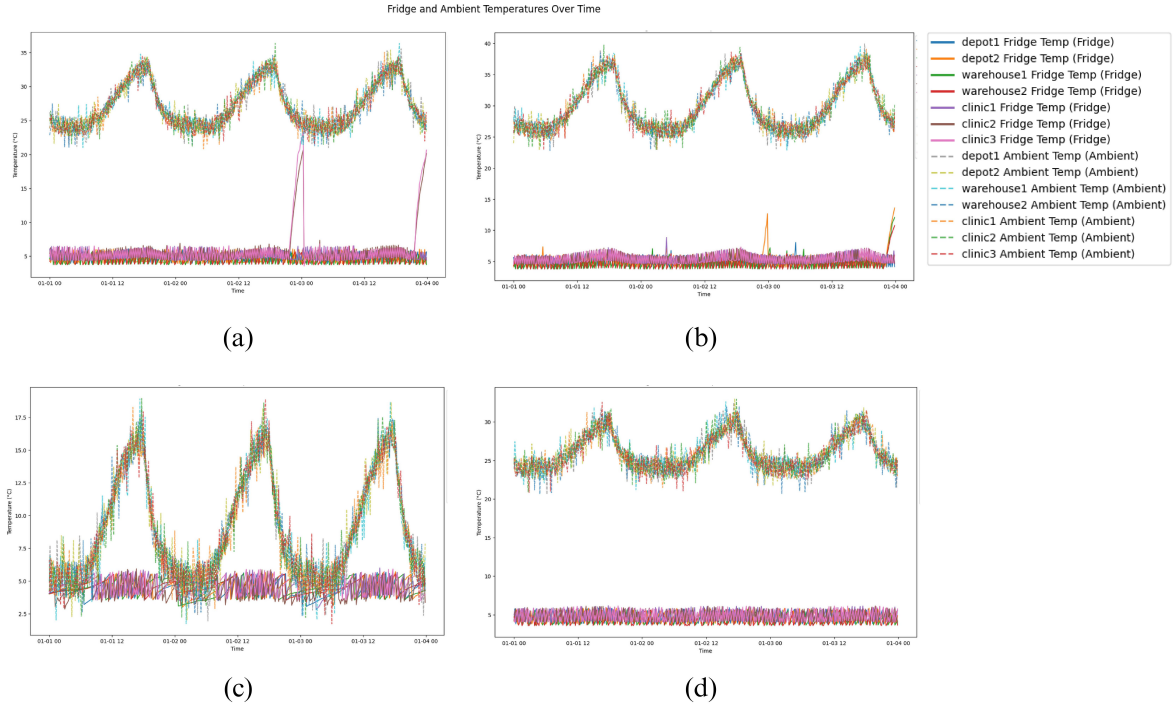

Figure 3: Ambient temperature profiles (dashed lines) and corresponding fridge internal temperatures (solid lines) across four simulated scenarios, (a) Gaza, (b) Sudan, (c) Nepal Highlands, and (d) post-earthquake Haiti, arranged in a 2×2 grid. Notably, panel (c) shows greater intraday fluctuations in ambient and fridge temperatures compared to the other scenarios, reflecting the large day–night swings characteristic of the Nepal Highlands.

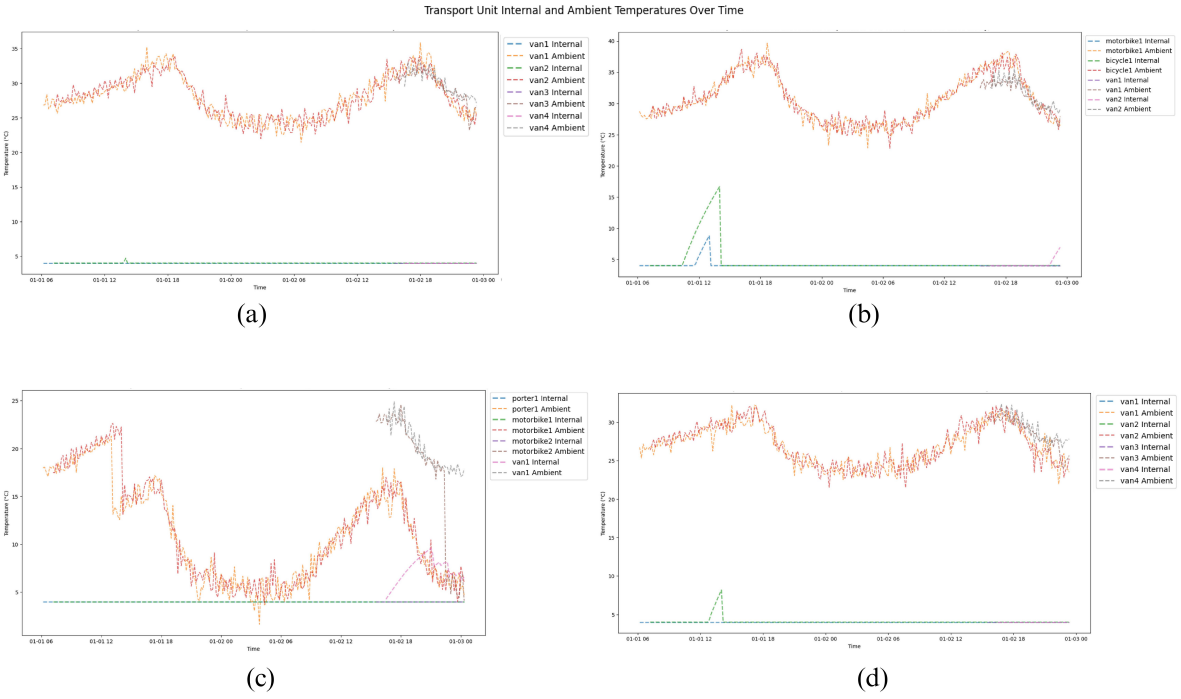

Figure 4: Ambient temperature profiles and corresponding transport unit internal temperatures across four simulated scenarios, (a) Gaza, (b) Sudan, (c) Nepal Highlands, and (d) post-earthquake Haiti, arranged in a 2×2 grid. While most transport units maintained safe 2–8 °C ranges, panel (b) shows a pronounced spike in bicycle temperatures after ice-pack depletion.

At the logistics level, two batches were successfully delivered to clinic1 and clinic2 through their respective warehouses and depots, while clinic3 received none due to intentional design constraints. With the exception of clinic 3, all multi-step handovers were completed without failure, with exposure accumulation recorded during transfers (Figure 5).

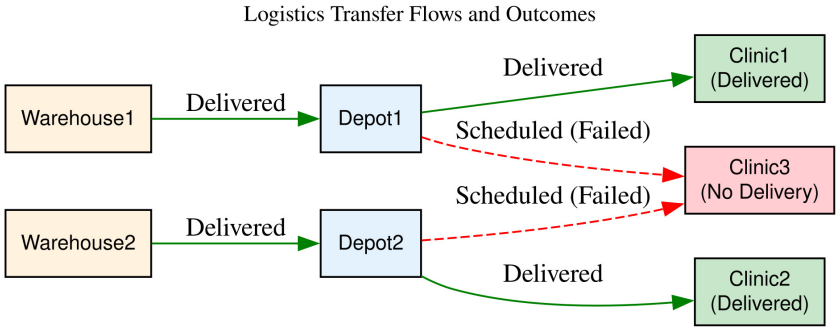

Figure 5: Transfer flows and outcomes for the baseline scenario. Two successful supply chains are shown from warehouses through depots to clinics, while the transfer to Clinic3 was intentionally pending/failed because only two batches were created.

Of the ten tracked medical items, only the Polio vaccine was expected to spoil. Its −20 °C storage requirement was incompatible with standard 2–8 °C refrigerators, leading to repeated spoilage across scenarios. All other items recorded minimal unsafe exposure hours, confirming that the modeled cold chain adequately preserved standard 2–8 °C products (Table 1).

Medical Item	**Outcome**
Measles Vaccine	Preserved
Polio (OPV)	Spoiled
Yellow Fever Vaccine	Preserved
Oral Cholera Vaccine	Preserved
Insulin	Preserved
Tetanus Toxoid	Preserved
Hepatitis B Vaccine	Preserved
Rabies Vaccine	Preserved
Antivenom	Preserved
Oxytocin	Preserved

Table 1: Preservation outcome of medical items across simulation runs.

Grid instability was the dominant disruption, comprising 18–25% of events with stochastic outages typically lasting 30–180 minutes (mean ~100 minutes). Gaza, Sudan, and Haiti showed the highest outage frequency, while Nepal remained relatively stable, reflecting predefined grid profiles. Power shortages frequently pushed facilities into critically low battery levels, particularly at depots and clinics. Although warehouses had the largest provisioning, they too reached zero reserves when inputs faltered. These conditions reflected stress-test assumptions rather than empirical outage patterns (Figure 6). Other disruptions included roadblocks, delays, and low-probability events such as tampering.

Overall, baseline configurations produced low spoilage but notable variation in temperature

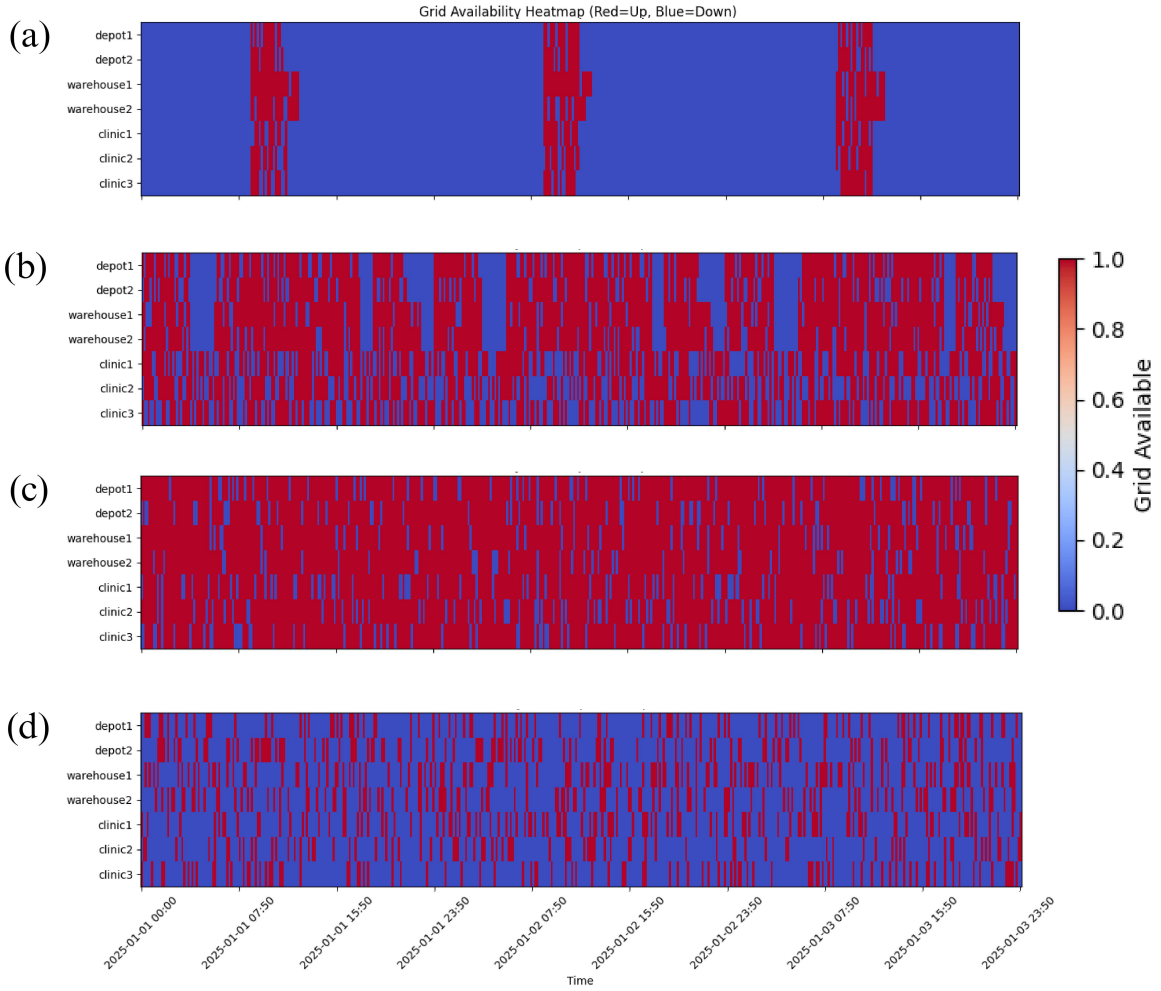

Figure 6: Heatmap of grid power availability across all four scenarios, (a) Gaza, (b) Rural Sudan, (c) Nepal Highlands, and (d) post-earthquake Haiti. Red indicates periods of grid availability, while blue indicates outages. Among the simulated contexts, Gaza (a) shows severe constraints with an imposed hourly availability profile, while Sudan (b) combines chronic unreliability with intermittent supply. Nepal (c) shows the highest relative grid reliability, although it is not perfect due to parameter assumptions, whereas Haiti (d) has low availability, reflecting the post-earthquake setting. Within each scenario, warehouses exhibit slightly better power stability compared to depots and clinics.

excursions and downtime. In Gaza, the baseline averaged 27 excursions and 30 downtime hours per node; only Resilient Grid and Power Upgrade interventions meaningfully improved outcomes, nearly halving both metrics. In Sudan, the baseline logged 12 excursions and over 22 hours downtime; Power Upgrade was the only effective intervention, reducing downtime, while fridge and transport upgrades not only failed to help, but they also worsened outcomes beyond baseline. In Nepal, baseline conditions were stable (9 hours downtime), and most interventions yielded no measurable gains. In post-earthquake Haiti, grid conditions remained highly unstable (16 downtime hours, 25 excursions); only Power Hardening and Infrastructure Shockproofing provided significant improvement, while other interventions showed little benefit.

Policy / Intervention	Temp Excursions	Downtime (h)	Δ vs. Baseline (Excursions / Downtime)
Baseline	27	30	–
Power Upgrade	16	19	−11 / −11
Behavior Change	27	30	0 / 0
Resilient Grid	14	19	−13 / −11
Fridge Upgrade	26	31	−1 / +1
Power Upgrade + Behavior Change	16	19	−11 / −11
Power Upgrade + Resilient Grid	9	11	−18 / −19
Power Upgrade + Fridge Upgrade	18	22	−9 / −8
Behavior Change + Resilient Grid	14	19	−13 / −11
Behavior Change + Fridge Upgrade	26	31	−1 / +1

Table 2: Intervention results for the Gaza clinic scenario. Performance of baseline and intervention scenarios, reported in terms of temperature excursions and downtime.

Policy / Intervention	Temp Excursions	Downtime (h)	Δ vs. Baseline (Excursions / Downtime)
Baseline	12	22	—
Power Upgrade	2	4	−10 / −18
Fridge Upgrade	15	26	+3 / +4
Robust Transport	11	19	−1 / −3
Power Upgrade + Robust Transport	2	4	−10 / −18
Fridge Upgrade + Robust Transport	15	25	+3 / +3
Power Upgrade + Fridge Upgrade	5	7	−7 / −15

Table 3: Intervention results for the Sudan rural scenario.

Policy / Intervention	Temp Excursions	Downtime (h)	Δ vs. Baseline (Excursions / Downtime)
Baseline	5	9	—
Warm Chain	5	9	0 / 0
Route Improved	5	9	0 / 0
Container Upgrade	5	9	0 / 0

Table 4: Intervention results for the Nepal highlands scenario.

Policy / Intervention	Temp Excursions	Downtime (h)	Δ vs. Baseline (Excursions / Downtime)
Baseline	16	25	—
Power Hardening	4	6	−12 / −19
Mobile Units	16	25	0 / 0
Infrastructure Shockproofing	12	19	−4 / −6
Community Training	16	25	0 / 0
Power Hardening + Mobile Units	4	6	−12 / −19
Power Hardening + Infrastructure Shockproofing	2	4	−14 / −21

Table 5: Intervention results for the Haiti post-earthquake scenario.

4 Discussion and Interpretation

This study introduced a modular simulation framework to examine the resilience of vaccine cold chains operating in humanitarian and resource-constrained settings. The framework integrates thermal dynamics, power variability, logistics, and human behavior to reveal how stresses accumulate within fragile supply systems. Across four scenarios, Gaza, Rural Sudan, Nepal Highlands, and post-earthquake Haiti, baseline configurations generally maintained safe storage ranges (2–8 °C) but consistently exposed vulnerabilities in last-mile clinics, low-insulation transport, and unstable power supply. Quantitatively, interventions that improved grid stability and energy reliability reduced temperature excursions and downtime by up to 60% compared with baseline configurations, whereas isolated hardware or behavioral changes produced little benefit and sometimes worsened outcomes. The framework is positioned as a stress-testing tool that surfaces structural fragilities under modeled assumptions, rather than a predictive model of real-world outcomes.

Although blackout frequencies were high and disruptions frequent, node-level temperatures did not collapse entirely because each facility was assumed to have access to multiple power modalities (grid, solar, battery, and generator), even if only at a limited scale. This redundancy provided minimal resilience and prevented uncontrolled warming.

Certain patterns were produced across all contexts. Clinics were the most vulnerable nodes, operating near the upper safety threshold due to limited insulation, frequent human interactions, and small power capacity. Power instability was the dominant source of stress, with outages generating temperature variability, battery depletion, and maladaptive responses even when spoilage did not occur. Transport robustness followed a clear hierarchy; moderately insulated carriers preserved stability, while lower insulation units experienced an increase in temperature. Finally, infrastructure-oriented interventions outperformed hardware upgrades, which underscores that fragility arises less from individual technical shortcomings than from systemic reliance on stable energy and logistics. Even without widespread spoilage, accumulated exposure hours, downtime, and failed deliveries highlighted points of systemic weakness with clear operational relevance.

The framework also illuminated systems-level dynamics. One theme was the layering of fragility, where power cuts triggered not only thermal excursions but also delayed repairs, disrupted deliveries, and increased likelihood of human error. Resilience thus emerged as

a property of interacting stresses rather than the absence of single failures. A second theme concerned the balance between centralized and decentralized strategies. Warehouses and depots benefited from stronger infrastructure and redundancy, while clinics relied on local autonomy but faced higher risks under unstable supply. This tension reflects a strategic dilemma over whether to invest in centralized robustness or distributed self-sufficiency. Finally, the modeled exclusion of one clinic illustrated the reality of resource triage under scarcity, where allocation choices carry unavoidable equity and ethical implications. Such dynamics are often invisible in simpler flow-based models yet critical for resilience and logistics planning in resource-limited systems.

Operationally, the results highlight the importance of context-specific interventions. In densely populated conflict-affected settings such as Gaza, ensuring energy reliability proved most impactful, while in rural Sudan, expanding solar or battery capacity offered the greatest benefit. In post-disaster Haiti, strategies that stabilized basic infrastructure reduced systemic fragility more effectively than technical upgrades at single nodes. Even in the relatively stable Nepal Highlands, improvements in transport and logistics reliability could add resilience despite overall system stability. These contrasts reinforce the need to align interventions with prevailing stresses rather than apply uniform solutions.

An unexpected finding was that, relative to the baseline, fridge upgrades alone worsened results by increasing both excursion and downtime. The benefit was negligible when paired with improvements to the generator and battery capacity and less than the gains from power upgrades alone. This counterintuitive result likely reflects a realistic interaction between larger, more powerful fridges and constrained backup systems. The net gain is limited since increased cooling capacity and thermal mass put more strain on batteries and generators, which are vulnerable to shallow reserves and refueling or charging delays. The results show that equipment enhancements are not guaranteed to result in universal gains and that their efficacy depends on the capacity and dependability of the supporting power system.

These insights may help advance understanding of how systemic stresses shape cold chain resilience, but they must be interpreted in the context of modeling assumptions. The next section discusses the framework's limitations and the need for further empirical validation.

4.1 Model Limitations and Assumptions

Several limitations of the present framework should be acknowledged. First, agent behaviors were represented as simplified probabilistic processes rather than calibrated from ethnographic or operational data. This allowed variability to be modeled but may not capture the full complexity of real-world practices. Second, the disruption engine reduced failures to stochastic triggers, whereas actual disruptions often arise from a combination of political tensions, bureaucratic delays, fuel shortages, regulatory dynamics, infrastructure damage, terrain constraints, seasonal disease outbreaks, and other context-specific factors. These variables interact in nonlinear ways that produce cascading effects beyond the reach of static simulations. Third, the evaluation metrics were restricted to spoilage, excursions, downtime, and deliveries. Other relevant dimensions, such as costs or secondary energy demands (e.g., lighting, computing, or non-cold-chain medical devices), were not included.

Fourth, the scenarios assumed the existence of at least minimal energy infrastructure, even when modeled with severe unreliability. However, some field reports describe even more

severe energy conditions, which include near-total grid collapse or the complete absence of formal supply in certain areas, particularly in Gaza, leading to cold chain continuity being impossible under any configuration. While the framework does permit nodes to be modeled without specific power sources, future work should more explicitly explore scenarios of complete absence. Fifth, the framework has not been empirically calibrated or validated against field data, as detailed monitoring records for crisis-affected regions remain scarce. The results should therefore be interpreted as stress-testing outputs that illustrate relative system behavior under assumed conditions rather than quantitative forecasts for specific regions. These constraints limit external generalizability but preserve internal validity for comparative scenario analysis.

4.2 Future Directions

The framework opens several directions for future research. The scope of the inventory model could be extended beyond vaccines to include blood supplies, biologics, or other temperature-sensitive commodities and linked to health outcome measures such as missed immunizations or projected outbreak risks. Climate-related stressors could be represented more explicitly, for example, by modeling prolonged heatwaves, storms, or flooding to capture climate change adaptation needs.

Another avenue is integration with established supply chain and transport optimization models. While conventional humanitarian logistics simulations emphasize flow and coverage, they rarely incorporate physics-based thermal dynamics or energy fragility. A hybrid approach could combine the strengths of optimization models with the framework's unique capabilities.

Sensitivity analysis showed that storage thermal properties dominate spoilage outcomes, while transport and technician parameters were less influential under baseline conditions. Future work could extend beyond one-at-a-time checks to explore multi-parameter interactions.

The modular architecture also supports scalability across different levels of analysis. Components can be applied to single-fridge assessments (e.g., performance under unreliable power at a node) or to large-scale network simulations. Because modules are interchangeable, the framework could be adapted to other infrastructure-dependent health systems beyond the cold chain. Finally, future development could improve usability and accessibility, for example, through clearer documentation, modular packaging, or user-friendly interfaces.

5 Conclusions

This study introduced a hybrid simulation framework that integrates thermal physics, power variability, human behavior, logistical disruptions, and temperature-dependent spoilage evaluation to assess cold chain resilience in humanitarian and resource-constrained contexts. Applied across four scenarios, the framework revealed that while systems generally preserved safe temperature ranges, fragilities were concentrated at the clinic level, in low-insulation transport, and wherever power supply was unstable.

Across scenarios, infrastructure-oriented interventions, particularly those improving grid stability and backup energy capacity, were consistently more effective than isolated equipment upgrades or behavioral changes. In several cases, conventional hardware improvements even degraded performance by increasing energy demand on fragile power systems. These results highlight that reliability depends not only on hardware specifications but on the broader

configuration of environmental, infrastructural, and behavioral interactions.

The framework provides a useful platform for stress-testing policy and technical modifications before field deployment. It allows for context-specific analysis of energy and logistics vulnerabilities and supports evidence-based planning for equitable access to temperature-sensitive medicines. While future work should include empirical calibration and broader metrics such as cost and health outcomes, this framework establishes a flexible and operationally grounded foundation for assessing resilience in fragile health infrastructure systems.

Funding
This research received no external funding.

Conflict of Interest
The author declares no conflict of interest.

Data and Code Availability
Supplementary materials, including spoilage verification results and intervention configuration details, are available on Zenodo at https://doi.org/10.5281/zenodo.17281048. The complete simulation codebase will be released through a public GitHub repository prior to journal submission.

References

[1] Advanco. The importance of the cold chain in the pharma industry - Advanco, 12 2024. URL https://www.advanco.com/article/the-importance-of-the-cold-chain-in-the-pharma-industry/.

[2] Mirai Intex. Pharma cold chain: pharmaceutical cold storage, managment and logstics, 11 2024. URL https://mirai-intex.com/blog/cold-chain-in-the-pharmaceutical-industry-ensuring-safe-and-effective-medications.

[3] World Health Organization: WHO. Close to one billion people globally are served by health-care facilities with no electricity access or with unreliable electricity, 1 2023. URL https://www.who.int/news/item/14-01-2023-close-to-one-billion-people-globally-are-served-by-health-care-facilities-with-no-electricity-access-or-with-unreliable-electricity.

[4] World Health Organization: WHO. Electricity in health-care facilities, 8 2023. URL https://www.who.int/news-room/fact-sheets/detail/electricity-in-health-care-facilities.

[5] Centers for Disease Control and Prevention. Vaccine storage and handling, 7 2024. URL https://www.cdc.gov/vaccines/hcp/storage-handling/index.html.

[6] United Nations Environment Programme. Why optimized cold-chains could save a billion COVID vaccines, 6 2020. URL https://www.unep.org/news-and-stories/story/why-optimized-cold-chains-could-save-billion-covid-vaccines.

[7] Irnela Bajrovic and Maria A. Croyle. Challenges in vaccine transport: can we deliver without the cold chain? *Expert Review of Vaccines*, 22(1):933–936, 10 2023. doi: 10.1080/14760584.2023.2273901. URL https://doi.org/10.1080/14760584.2023.2273901.

[8] Aaron S. Wallace, Kong Krey, John Hustedt, Eleanor Burnett, Narin Choun, Danni Daniels, Margaret L. Watkins, Sann Chan Soeung, and Richard Duncan. Assessment of vaccine wastage rates, missed opportunities, and related knowledge, attitudes and practices during introduction of a second dose of measles-containing vaccine into Cambodia's national immunization program. *Vaccine*, 36(30):4517–4524, 6 2018. doi: 10.1016/j.vaccine.2018.06.009. URL https://doi.org/10.1016/j.vaccine.2018.06.009.

[9] World Health Organization. How to Develop a Continuous Improvement Plan (cIP), 2018. URL https://iris.who.int/bitstream/handle/10665/272861/9789241514293-eng.pdf.

[10] Médecins Sans Frontières. Heat-stable vaccines urgently needed to reach the one in five children missed by immunisation worldwide, 4 2014. URL https://www.msf.org/heat-stable-vaccines-urgently-needed-reach-one-five-childre n-missed-immunisation-worldwide.

[11] Diriba Feyisa, Fikadu Ejeta, Temesgen Aferu, and Oliyad Kebede. Adherence to WHO vaccine storage codes and vaccine cold chain management practices at primary healthcare facilities in Dalocha District of Silt'e Zone, Ethiopia. *Tropical Diseases Travel Medicine and Vaccines*, 8(1), 4 2022. doi: 10.1186/s40794-022-00167-5. URL https://doi.org/10.1186/s40794-022-00167-5.

[12] Reetika Malik Yadav, Mangala Gomare, Arun Gaikwad, Upalimitra Waghmare, Utkarsh Betodkar, Meeta Dhaval Vashi, Vineet Kumar Kamal, Jeromie Wesley Vivian Thangaraj, Sampada Bangar, Tarun Bhatnagar, and Manoj Murhekar. Interplay of missed opportunity for vaccination and poor response to the vaccine led to measles outbreak in a slum area of Eastern Mumbai, India. *Epidemiology and Infection*, 152, 1 2024. doi: 10.1017/s0950268824000426. URL https://doi.org/10.1017/s0950268824000426.

[13] Daryl Newcombe. Fridge failure spoils $133,000 worth of non-COVID vaccines at MLHU, 11 2024. URL https://www.ctvnews.ca/london/article/fridge-failure-spoils-133000-wor th-of-non-covid-vaccines-at-mlhu.

[14] E. Weir. Preventing cold chain failure: vaccine storage and handling. *Canadian Medical Association Journal*, 171(9):1050, 10 2004. doi: 10.1503/cmaj.1041565. URL https://doi.org/10.1503/cmaj.1041565.

[15] Lina Hemmeda, Alaa S. Ahmed, and Maram Omer. Sudan's armed rivalry: A comment on the vulnerable healthcare system catastrophe. *Health Science Reports*, 6(8), 8 2023. doi: 10.1002/hsr2.1517. URL https://doi.org/10.1002/hsr2.1517.

[16] Lina Hemmeda, Angad Tiwari, Barakat Olajumoke Kolawole, Fathima Shehnaz Ayoobkhan, Kainat Fatima, Moshi Moshi Shabani, Mrinmoy Kundu, NagaSpurthy Reddy Anugu, Riya Mary Richard, Danya Ibrahim, and Khabab Abbasher Hussien Mohamed Ahmed. The critical pharmaceutical situation in sudan 2023: A humanitarian catastrophe

of civil war. *International Journal for Equity in Health*, 23(1), March 2024. doi: 10.1186/s12939-024-02103-9. URL https://doi.org/10.1186/s12939-024-02103-9.

[17] Save the Children. Sudan: Lifesaving vaccines for children destroyed in power outages amidst violence, 4 2023. URL https://www.savethechildren.net/news/sudan-lifesaving-vaccines-children-destroyed-power-outages-amidst-violence.

[18] UNICEF. Enhancing immunization programmes in Yemen, 12 2019. URL https://www.unicef.org/yemen/stories/enhancing-immunization-programmes-yemen.

[19] Medical Product Quality Report – COVID-19 issues. Issue 14, October, November December 2021. Technical report, 2021. URL https://www.iddo.org/document/medical-product-quality-report-covid-19-issues-issue-14-april-2022-data-october-december.

[20] OCHA. Occupied Palestinian Territory (FA) 2023 Flash Appeal: from 01/10/2023 to 31/12/2023, 10 2023. URL https://humanitarianaction.info/plan/1186/article/opt-fa-2023.

[21] Human Rights Watch. Israel and Palestine: Events of 2023, 2024. URL https://www.hrw.org/world-report/2024/country-chapters/israel-and-palestine.

[22] OCHA. Humanitarian situation Update 300: Gaza Strip. Technical report, 6 2025. URL https://www.ochaopt.org/content/humanitarian-situation-update-300-gaza-strip.

[23] Ayah Mohammed, Patrick James, and AbuBakr Bahaj. Electricity access linkages to sustainable development goals in rural Sudan. *Sustainability*, 17(6):2441, 3 2025. doi: 10.3390/su17062441. URL https://doi.org/10.3390/su17062441.

[24] CarbonCopy. Climate change can impact vaccine efficacy, safety and access: Study, 12 2024. URL https://carboncopy.info/climate-change-can-impact-vaccine-efficacy-safety-and-access-study/.

[25] Kai Zhang, Yifang Dang, Yiming Li, Cui Tao, Junguk Hur, and Yongqun He. Impact of climate change on vaccine responses and inequity. *Nature Climate Change*, 14(12): 1216–1218, 11 2024. doi: 10.1038/s41558-024-02192-y. URL https://doi.org/10.1038/s41558-024-02192-y.

[26] UNRWA. UNRWA Situation Report 184 on the humanitarian crisis in the Gaza Strip and the West Bank, including East Jerusalem, 8 2025. URL https://www.unrwa.org/resources/reports/unrwa-situation-report-184-situation-gaza-strip-and-west-bank-including-east-jerusalem.

[27] Ajit Niranjan. 'Hellish': heatwave brings hottest nights on record to the Middle East. 8 2025. URL https://www.theguardian.com/world/2025/aug/15/hellish-heatwave-brings-hottest-nights-on-record-to-the-middle-east.

[28] Climate Centre. Sudan. Technical report, 2024. URL https://www.climatecentre.org/wp-content/uploads/RCCC-Country-profiles-Sudan-2024_final.pdf.

[29] Nepal Tourism Board. Climate in Nepal. URL https://ntb.gov.np/plan-your-trip/about-nepal/climate.

[30] Weather Spark. Summer weather in Port-au-Prince Haiti. URL https://weatherspark.com/s/25360/1/Average-Summer-Weather-in-Port-au-Prince-Haiti.

[31] Damilola Jeremiah Ayowole, Glory Olalekan Adebajo, Toheeb Omobolaji Lasisi, and Jinod Gbolahan Bakai. Effects of climate change on vaccine storage and cold chain logistics: a qualitative study in Ogun State, Nigeria. *BMJ Global Health*, 10(7):e018990, 7 2025. doi: 10.1136/bmjgh-2025-018990. URL https://doi.org/10.1136/bmjgh-2025-018990.

[32] AKCP. Preventing Cold Chain Failures using Remote Monitoring Systems, 1 2021. URL https://www.environmental-expert.com/articles/preventing-cold-chain-failures-using-remote-monitoring-systems-1012416.

[33] David Gligor, Albert Tan, and Thi Nha Trang Nguyen. The obstacles to cold chain implementation in developing countries: insights from Vietnam. *The International Journal of Logistics Management*, 29(3):942–958, 6 2018. doi: 10.1108/ijlm-02-2017-0026. URL https://doi.org/10.1108/ijlm-02-2017-0026.

[34] Leslie E. Mueller, Leila A. Haidari, Angela R. Wateska, Roslyn J. Phillips, Michelle M. Schmitz, Diana L. Connor, Bryan A. Norman, Shawn T. Brown, Joel S. Welling, and Bruce Y. Lee. The impact of implementing a demand forecasting system into a low-income country's supply chain. *Vaccine*, 34(32):3663–3669, 5 2016. doi: 10.1016/j.vaccine.2016.05.027. URL https://doi.org/10.1016/j.vaccine.2016.05.027.

[35] Bruce Y. Lee, Leila A. Haidari, Wendy Prosser, Diana L. Connor, Ruth Bechtel, Amelia Dipuve, Hidayat Kassim, Balbina Khanlawia, and Shawn T. Brown. Re-designing the Mozambique vaccine supply chain to improve access to vaccines. *Vaccine*, 34(41): 4998–5004, 8 2016. doi: 10.1016/j.vaccine.2016.08.036. URL https://doi.org/10.1016/j.vaccine.2016.08.036.

[36] Leila A. Haidari, Diana L. Connor, Angela R. Wateska, Shawn T. Brown, Leslie E. Mueller, Bryan A. Norman, Michelle M. Schmitz, Proma Paul, Jayant Rajgopal, Joel S. Welling, Jim Leonard, Sheng-I Chen, and Bruce Y. Lee. Augmenting Transport versus Increasing Cold Storage to Improve Vaccine Supply Chains. *PLoS ONE*, 8(5):e64303, 5 2013. doi: 10.1371/journal.pone.0064303. URL https://doi.org/10.1371/journal.pone.0064303.

[37] Eyüp Ensar Işık and Seyda Topaloglu Yildiz. Optimizing the COVID-19 cold chain vaccine distribution network with medical waste management: A robust optimization approach. *Expert Systems with Applications*, 229:120510, 5 2023. doi: 10.1016/j.eswa.2023.120510. URL https://doi.org/10.1016/j.eswa.2023.120510.

[38] Yanju Chen, Mengxuan Chen, and Tianran Hu. Designing a sustainable-resilient vaccine cold chain network in uncertain environments. *Computers Chemical Engineering*, page 108936, 11 2024. doi: 10.1016/j.compchemeng.2024.108936. URL https://doi.org/10.1016/j.compchemeng.2024.108936.

[39] Saeedeh Khalilpoor, Mehdi A. Kamran, and Maghsud Solimanpur. Resilient COVID-19 vaccine supply chain: An optimization and simulation approach for multi-objective management. *Transportation Research Part E Logistics and Transportation Review*, 201:104168, 7 2025. doi: 10.1016/j.tre.2025.104168. URL https://doi.org/10.1016/j.tre.2025.104168.

[40] Bahareh Kargar, Pedram MohajerAnsari, İ. Esra Büyüktahtakın, Hamed Jahani, and Sri Talluri. Data-driven modeling for designing a sustainable and efficient vaccine supply chain: A COVID-19 case study. *Transportation Research Part E Logistics and Transportation Review*, 184:103494, 3 2024. doi: 10.1016/j.tre.2024.103494. URL https://doi.org/10.1016/j.tre.2024.103494.

[41] Zhile Wang and Jihai Zhang. Agent-based evaluation of humanitarian relief goods supply capability. *International Journal of Disaster Risk Reduction*, 36:101105, 2 2019. doi: 10.1016/j.ijdrr.2019.101105. URL https://doi.org/10.1016/j.ijdrr.2019.101105.

[42] UNICEF. Echnical Review of Public Health Supply Chain Assessment tools: An analysis of major supply chain assessment tools and approaches. URL https://www.unicef.org/supply/documents/technical-review-public-health-supply-chain-assessment-tools.

[43] UNICEF. Supply Chain Maturity Model Concept Note, 2021. URL https://www.unicef.org/supply/documents/supply-chain-maturity-model-concept-note.

[44] Megan Hay, Anika Teichert, Sarah Kilz, and Agnes Vosen. Resilience in the Vaccine Supply Chain: Learning from the COVID-19 Pandemic. *Vaccines*, 13(2):142, 1 2025. doi: 10.3390/vaccines13020142. URL https://doi.org/10.3390/vaccines13020142.

[45] World Health Organization. Effective Vaccine Management (EVM). URL https://www.who.int/teams/immunization-vaccines-and-biologicals/essential-programme-on-immunization/supply-chain/effective-vaccine-management-(evm).

[46] Didier Clénet. Accurate prediction of vaccine stability under real storage conditions and during temperature excursions. *European Journal of Pharmaceutics and Biopharmaceutics*, 125: 76–84, 1 2018. doi: 10.1016/j.ejpb.2018.01.005. URL https://doi.org/10.1016/j.ejpb.2018.01.005.

[47] Cristiana Campa, Thierry Pronce, Marilena Paludi, Jos Weusten, Laura Conway, James Savery, Christine Richards, and Didier Clénet. Use of stability modeling to support accelerated vaccine development and supply. *Vaccines*, 9(10):1114, 9 2021. doi: 10.3390/vaccines9101114. URL https://doi.org/10.3390/vaccines9101114.

[48] David Jenkins, Aida Cancel, and Thomas Layloff. Mean kinetic temperature evaluations through simulated temperature excursions and risk assessment with oral dosage usage for health programs. *BMC Public Health*, 22(1), 2 2022. doi: 10.1186/s12889-022-12660-9. URL https://doi.org/10.1186/s12889-022-12660-9.

[49] K De Boeck C Decouttere Nico Vandaele. Vaccine distribution supply chains in developing countries: A literature review. *ideas.repec.org*, 11 2018. URL https://ideas.repec.org/p/ete/kbiper/629348.html.

[50] Coordination of Humanitarian Affairs. Electricity in the Gaza Strip | United Nations Office for the Coordination of Humanitarian Affairs - Occupied Palestinian Territory. URL https://www.ochaopt.org/page/gaza-strip-electricity-supply.

[51] Hanrui Cao, Xi Li, Samir Belabbes, Luca Dell'oro, and Changyong Dou. Estimates of power supply during the 2023 Gaza humanitarian crisis using night-time light images.

Geo-spatial Information Science, pages 1–19, 1 2025. doi: 10.1080/10095020.2024.2439387. URL https://doi.org/10.1080/10095020.2024.2439387.

[52] United Nations. GAZA / ELECTRICITY CRISIS, 2 2025. URL https://media.un.org/unifeed/en/asset/d333/d3334996.

[53] Wikipedia contributors. Electricity crisis in the Gaza Strip, 9 2025. URL https://en.wikipedia.org/wiki/Electricity_crisis_in_the_Gaza_Strip.

[54] Office for the Coordination of Humanitarian Affairs. Humanitarian Situation Update 326 | Gaza Strip, 9 2025. URL https://www.unocha.org/publications/report/occupied-palestinian-territory/humanitarian-situation-update-326-gaza-strip.

[55] UNICEF. 3 major obstacles to delivering aid in Gaza, 1 2024. URL https://www.unicef.org/stories/3-major-obstacles-delivering-aid-gaza.

[56] Kenta Usui. Concept Project Information Document (PID) - Sudan Energy Transition and Access Project - P175040. URL https://documents.banquemondiale.org/fr/publication/documents-reports/documentdetail/702241600887137438/concept-project-information-document-pid-sudan-energy-transition-and-access-project-p175040.

[57] Razaz H. Basheir and Mohamed Salah Abdelrahman. *The electricity crisis in Sudan:*. 10 2023. doi: 10.2307/jj.7583922.12. URL https://doi.org/10.2307/jj.7583922.12.

[58] United Nations News. Sudan: UN warns of soaring displacement and looming floods, 7 2025. URL https://news.un.org/en/story/2025/07/1165176.

[59] International Federation of Red Cross and Red Crescent Societies (IFRC). Sudan Floods 2024 - DREF Operation (MDRSD034), 9 2024. URL https://reliefweb.int/report/sudan/sudan-floods-2024-dref-operation-mdrsd034.

[60] Nepal News. Landslides block six major roads across Nepal, 6 2025. URL https://english.nepalnews.com/s/nation/landslides-block-six-major-roads-across-nepal/.

[61] The Kathmandu Post. Araniko Highway closed for 11 days due to landslides, 8 2025. URL https://kathmandupost.com/national/2025/08/13/araniko-highway-closed-for-11-days-due-to-landslides.

[62] Wikipedia contributors. Electricity sector in Haiti, 9 2025. URL https://en.wikipedia.org/wiki/Electricity_sector_in_Haiti.